coatings

MDPI

Review

Review on the Solar-Driven Photocathodic Protection of Metals in the Marine Environment

Mingbo Yang [1], Ruizhe Jiang [1], Jinke Zhu [1], Xuan Zhang [1], Guidong Li [1], Weitao Li [1], Fubin Ma [2,3,*], Xueqing Jiang [1] and Hong Li [1,*]

[1] College of Mechanical and Electrical Engineering, Qingdao University, Qingdao 266071, China; 15953718142@163.com (M.Y.); 18953249359@163.com (R.J.); 17854273885@163.com (J.Z.); jiangxq2023@163.com (X.J.)
[2] State Key Laboratory of Bio-Fibers and Eco-Textiles, Qingdao University, Qingdao 266071, China
[3] Open Studio for Marine Corrosion and Protection, Pilot National Laboratory for Marine Science and Technology, Qingdao 266237, China
* Correspondence: mafubin2024@163.com (F.M.); lhqdio1987@163.com (H.L.); Tel.: +86-532-85953679 (F.M.)

Abstract: Photocathodic protection (PCP) technology has gained wide attention in the field of corrosion due to its green, environmentally friendly, and sustainable characteristics, and has become a protection technology with broad development prospects in the future marine environment. By investigating recent research results, the mainstream photoanode materials are TiO_2, $BiVO_4$, g-C_3N_4, ZnO, In_2O_3, $SrTiO_3$ and other materials. Among them, TiO_2 is an ideal photoanode material for PCP because of its efficient photochemical corrosion resistance, remarkable reaction stability, and excellent photoelectric properties. However, TiO_2 itself has more drawbacks, such as limited utilization of visible light and low photogenerated electron-hole separation efficiency. These defects limit the wide application of TiO_2 in PCP. Through modification methods, the reaction efficiency can be substantially improved and the availability of TiO_2 can be increased. This paper lists the research progress of modifying TiO_2 materials using metal and non-metal doping modification, semiconductor compounding technology, and energy storage materials for application in PCP, and introduces several new types of photoanode materials. This paper suggests new ideas for the design of more efficient photoanodes.

Keywords: photocathodic protection; corrosion; TiO_2; stainless steel; carbon steel

check for updates

Citation: Yang, M.; Jiang, R.; Zhu, J.; Zhang, X.; Li, G.; Li, W.; Ma, F.; Jiang, X.; Li, H. Review on the Solar-Driven Photocathodic Protection of Metals in the Marine Environment. *Coatings* **2024**, *14*, 276. https://doi.org/10.3390/coatings14030276

Academic Editor: Chi Tat Kwok

Received: 29 December 2023
Revised: 5 February 2024
Accepted: 22 February 2024
Published: 25 February 2024

Copyright: © 2024 by the authors. Licensee MDPI, Basel, Switzerland. This article is an open access article distributed under the terms and conditions of the Creative Commons Attribution (CC BY) license (https://creativecommons.org/licenses/by/4.0/).

1. Introduction

As the marine economy continues to thrive, there is a growing annual demand for metals owing to their affordability and reliability. In contrast, metal corrosion presents a significant challenge in the metal industry and related products, especially in marine and other saline environments [1,2]. Various anti-corrosion approaches have been suggested, encompassing corrosion inhibitors [3], anticorrosion coatings [4], and electrochemical protection [5]. Notably, photo-electro-chemical cathodic protection (PCP) has garnered growing interest due to its environmentally sustainable and energy-saving benefits. Solar-driven anti-corrosion technology (PCP) has become a prominent research area of marine metal protection [6].

The principle of the PCP technique is shown in Figure 1. There are two forms of PCP technology in application. One is to coat the semiconductor on the exterior of the safeguarded metal [7], and the other is to connect the semiconductor material to the protected metal as a photoanode [8–10]. Under solar light irradiation, when the energy provided by the natural light (hv) is larger than the forbidden bandwidth of the photoanode, the electrons situated in the valence band (VB) will absorb the energy from photons and undergo excitation to jump to the conduction band (CB), producing photogenerated electrons (e^-) and photogenerated holes (h^+). At this time, under the influence of the

space electric field, photogenerated holes migrate to the semiconductor surface, and the oxidation reaction occurs with the electron donor OH^- or H_2O in the solution. Parts of the photogenerated electrons are compounded with the holes and parts of the electrons are transferred to the metal to which they are connected. In this process, the semiconductor is used as a photoanode that can generate photogenerated electrons and the photogenerated electrons are moved onto the coupling metal so that the metal surface potential decreases, thereby effectively inhibiting metal corrosion.

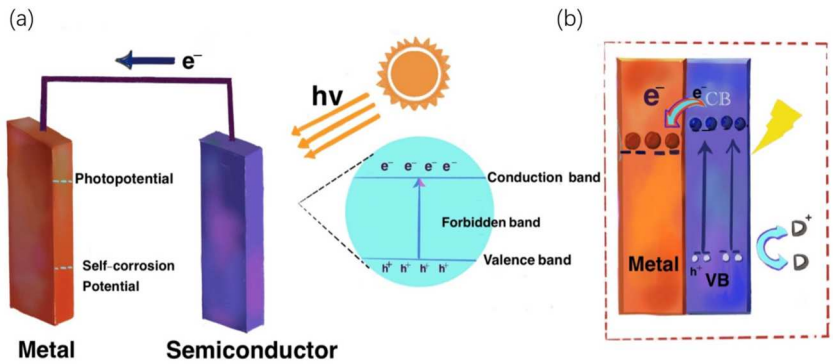

Figure 1. Schematic diagram of PCP technology. (**a**) form one; (**b**) form two.

2. PCP Properties of TiO_2-Based Photoelectrodes

TiO_2 nanomaterials are often used as photoanode materials for PCP because of their outstanding photoelectric characteristics and remarkable stability, but there are still many critical defects to be overcome for their pFractical applications. Firstly, the forbidden bandwidth (~3.2 eV) of TiO_2 is too wide, resulting in low utilization of visible light, and it can only respond to ultraviolet (UV) light at a wavelength of $\lambda < 387$ nm. In addition, the photogenerated carriers in pure TiO_2 are easily compounded, which prevents them from providing PCP for metals in dark conditions [11]. For this reason, TiO_2 has been modified to broaden its capacity to absorb light into the visible spectrum. The structure of the semiconductor is modulated to inhibit the photogenerated electron-hole complexation, thus, improving the electron utilization. Li et al. [12] tuned the ratio of TiO_2 crystal surface on the F-doped Tin Oxide (FTO) substrate by changing the growth angle and a meshed TiO_2 film exhibiting superior photoelectric conversion efficiency was achieved. The orientation of the FTO concerning the lower surface was modified using a fixture, as illustrated in Figure 2. All TiO_2 films grown at different angles exhibited a plate-like morphology, each with a thickness ranging from 50 to 100 nm. TiO_2-60° exhibits the best photovoltaic conversion efficiency due to the exposed area of the TiO_2 (101) crystal surface.

The current modifications of TiO_2 include metal element doping, non-metallic element doping, semiconductor composite, and shape control. These modified TiO_2 methods are expected to improve the utilization of TiO_2 for solar energy, photo-generated carrier separation efficiency, and continuous protection in the dark state, thus, providing new ideas and methods for the application of modified composites in the field of PCP.

2.1. Metal and Non-Metal Doping Modification

Metal and non-metal doping modification is one of the hot spots in TiO_2 modification research. Metal (e.g., Fe, Ni, Cr, W) doping causes TiO_2 to interact with metal ions under high temperature treatment, thus, changing the semiconductor lattice and extending the wavelength range of visible light absorption by TiO_2. Liu et al. [13] prepared Fe-doped TiO_2 films. Under white light irradiation, the photo-electro-chemical properties of Fe-doped TiO_2 films were significantly enhanced compared with those of TiO_2 films. Eshaghzadeh et al. [14] doped TiO_2 with Fe and Cr and found that the Fe and Cr co-doping inhibited the recombination of charge carriers in TiO_2. Sun et al. [15] prepared Ni-doped TiO_2 photoanodes, and found that the Ni doping extended the edge of the absorption band of TiO_2 to the visible range (420–520 nm). This is mainly attributed to the substitution

of Ti^{4+} lattice sites by Ni, which leads to the formation of oxygen vacancies and, thus, improves the photo-generated electron transfer rate. Momeni et al. [16] have employed a one-step anodic oxidation method to simultaneously incorporate different proportions of tungsten and iron into TiO_2 nanotubes for PCP of metals. The experimental results indicate that the Ti, O, W, and Fe elements have been uniformly distributed on the surfaces of the samples. The tungsten-iron-doped TiO_2 nanotubes effectively protect 403 stainless steel (SS) from corrosion. Under visible light irradiation, the tungsten-iron-TiO_2 samples with equal proportions of tungsten and iron exhibit the best photo-electro-chemical corrosion protection performance for SS. Momeni et al. [17] used a single-step anodic oxidation method to modulate the ratio of W–Cr by changing the electrolyte composition. Compared with pure TiO_2, the co-doping of W–Cr can stimulate more electron generation and have a certain inhibition effect on the recombination of TiO_2 carriers, resulting in a greater current density after co-doping, as well as a great reduction of the corrosion potential of 403 SS, which indicate the improvement of the PCP performance of TiO_2 by W–Cr co-doping.

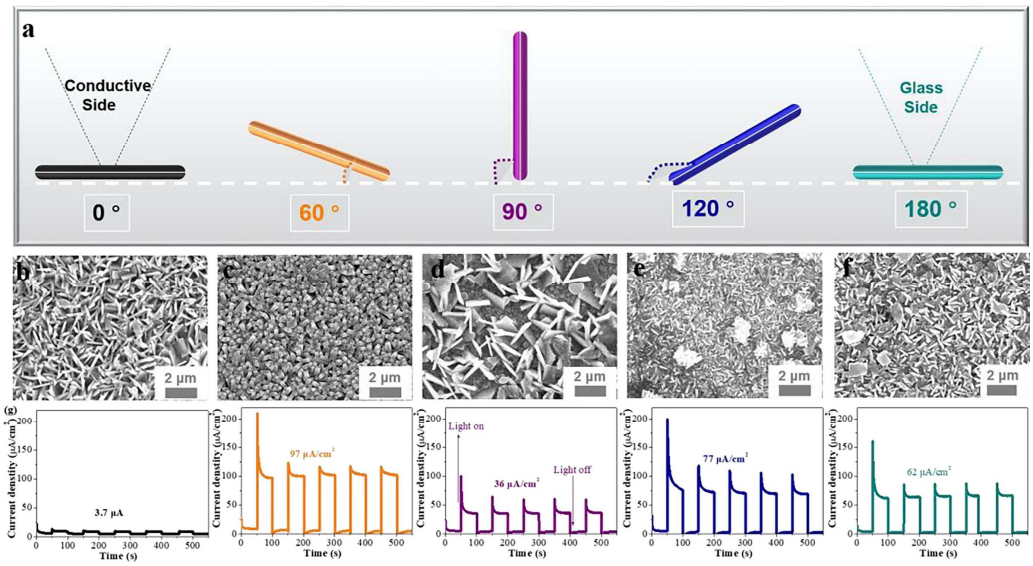

Figure 2. (**a**) Schematic of TiO_2 nanotubes, (**b**–**f**) SEM photographs, and (**g**) photocurrent-time curves (0°, 60°, 90°, 120°, and 180° from left to right, respectively) [12].

The principle of TiO_2 doping by non-metals (N, B, S, C, etc.) is based on the hybridization of the 2p-orbitals of O in TiO_2 with the p-orbitals of non-metals. This leads to a shift in the valence band of TiO_2, a decrease in the forbidden band width, and an increase in the utilization efficiency of light. Li et al. [18] prepared N-doped nanoflowering TiO_2 films. The absorption edge of the N-doped TiO_2 film obtained through hydrothermal treatment for 12 h appeared around 650 nm, with the corresponding bandwidth estimated to be 1.91 eV, significantly smaller than that of pure TiO_2. Fe, Cu, and N co-doped TiO_2 nanopowders have high photo-catalytic activity under visible light [19]. Zhou et al. [20] prepared carbon quantum dot-modified anatase/rutile TiO_2 photoanodes. Compared with pure TiO_2, the charge separation efficiency and surface charge injection efficiency of the modified TiO_2 photoanodes were greatly improved. Among them, the carbon quantum dots played a role in improving the oxygen precipitation reaction kinetics of TiO_2 as well as broadening the visible light absorption range of TiO_2. Lei et al. [21] reported that N and F co-doped TiO_2 thin films can negatively shift the potential of 304 SS from 55 mV to −460 mV, which improves the PCP effect of TiO_2. Arman et al. [22] prepared S-doped TiO_2 thin films. The best performance of TiO_2 thin films was obtained at 10% S doping concentration and 450 °C roasting temperature. This is due to the fact that sulfur ions are incorporated into the internal lattice of TiO_2, and the photo-electric conversion performance of TiO_2 films is significantly improved. Momeni et al. [23] successfully prepared B/TiO_2 nanotubes with different boron contents using a one-step anodic oxidation method and

evaluated the photo-electro-chemical protection effect of the prepared B/TiO_2 composite on 403 SS. The results showed that B doping boosted the photo-catalytic activity of TiO_2 under visible light exposure, as well as the photo = electro-chemical protection effect on 403 SS. Momeni et al. [24] found that the co-doping of W–Cr can stimulate more electron generation and have a certain inhibition effect on the recombination of TiO_2 carriers, resulting in a greater current density after co-doping, as well as a great reduction of the corrosion potential of 403 SS. Table 1 shows the photo-electro-chemical protection performance of different metal and non-metal doped TiO_2 materials.

Table 1. Comparison of PCP performances of different metal and non-metal doped TiO_2 materials.

Doped Metal/Non-Metal	Metal	Light Source	Potential Drop/mV	Reference
Fe	304 SS	White light	270	[13]
Ni	304 SS	Visible light	550	[15]
W-Fe	403 SS	Visible light	370	[16]
W–Cr	403 SS	Visible light	400	[17]
N	304 SS	Visible light	270	[18]
N-F	304 SS	Visible light	250/450	[21]
S	304 SS	Visible light	225	[22]
B	403 SS	Visible light	395	[23]
Fe-N-S	403 SS	White light	413	[24]

2.2. Semiconductor Compounding Technology

The combination of narrow bandgap semiconductors with TiO_2 leads to overlapping energy levels due to the difference in band structure and bandgap width between the two semiconductors, resulting in a decrease in the recombination rate of electron-hole pairs in TiO_2. Table 2 shows the PCP performances of some semiconductor composite TiO_2 materials. Zhang et al. [25] successfully synthesized SnO_2/TiO_2 nanorod composite films with enhanced PCP performance and electron storage capacity through hydrothermal treatment and electro-deposition. Compared to pure TiO_2 nanorod films, SnO_2/TiO_2 nanorod composite films exhibit excellent photoresponse capability and photo-electro-chemical efficiency. By depositing SnO_2 nanoparticles, the photocurrent density of this composite film is nearly three times higher than that of pure TiO_2 nanorods. Compared to the original TiO_2 nanorod film, the SnO_2/TiO_2 nanorod film shows outstanding cathodic protection performance on 304 SS in a 0.5 mol/L NaCl solution under white light illumination. Furthermore, the SnO_2/TiO_2 nanorod film can achieve delayed protection even after light is turned off due to the electron storage characteristics of SnO_2. Guan et al. [26] successfully fabricated highly efficient composite thin film photoanodes on conductive glass substrates by employing a three-step synthesis method, involving hydrothermal reaction and chemical vapor deposition, to co-modify rutile TiO_2 nanorods with g-$C_3N_4/SrTiO_3$. In comparison to unmodified TiO_2 films, the g-$C_3N_4/SrTiO_3/TiO_2$ composite films exhibited a significantly improved absorption of visible light, leading to a 4.5-fold increase in photocurrent density. This improvement is attributed to the heightened separation and transfer efficiency of photo-generated electron-hole pairs. Under white light illumination, the composite film photoanode lowered the potential of coupled 403 SS in a 0.5 M NaCl solution by 680 mV, showcasing a markedly enhanced effect of photo-electro-chemical cathodic protection. Li et al. [27] successfully prepared a novel $In_2S_3/Ag_2S/TiO_2$ nanotube array using continuous ion layer adsorption and electrochemical anodic oxidation methods and applied it as a photoanode for photo-electro-chemical cathodic protection. The study showed that compared to pure TiO_2, the $In_2S_3/Ag_2S/TiO_2$ nanocomposite exhibited better photoelectrocatalytic and photo-electro-chemical cathodic protection performance. The photocurrent potential of Q235 carbon steel coupled with $In_2S_3/Ag_2S/TiO_2$ shifted to a negative value of 0.92 V relative to SCE under illumination, and the photocurrent density reached 211 μA cm^{-2}, which was approximately 4.5 times that of TiO_2. Han et al. [28] synthesized NiO/TiO_2 p-n heterojunction composite materials through chemical plating

and annealing, leading to TiO_2 nanotube arrays adorned with a layer of NiO particles. The study showed that under visible light irradiation, the open circuit potential of 304 SS coupled with NiO/TiO_2 in a 3.5% NaCl solution can reach −760 mV, while the open circuit potential of 304 SS coupled with TiO_2 is only −330 mV. The NiO/TiO_2 heterojunction composite material exhibits excellent cathodic protection performance. Wang et al. [29] prepared layer-by-layer assembled TiO_2 nanotubes/SnO_2 quantum dots/Ag nanoparticles on titanium foil by anodic oxidation/hydrothermal/pulsed electrodeposition to obtain Ag/SnO_2 co-modified TiO_2 composite photoanodes, which have power storage capacity and good photocathodic protection performance. Due to the surface plasmon resonance (SPR) effect of Ag, Ag nanoparticles are photo-excited to generate electrons, which are then transferred to the conduction band of TiO_2, thus, promoting charge separation and transfer efficiency. Ma et al. [30] prepared MoS_2 microsphere/TiO_2 nanotube nanocomposites by a two-step anodic oxidation-hydrothermal method. By coating MoS_2 on the surface of TiO_2 nanotubes, the absorption area for visible light is broadened and the absorption density in the visible light region is increased, facilitating the utilization of visible light. The MoS_2 and TiO_2 interface forms an effective heterojunction electric field, significantly enhancing the separation efficiency of photo-generated electron-hole pairs and prolonging the lifetime of photo-generated electrons. The results demonstrate the significant PCP effect of MoS_2/TiO_2 on 304 SS under visible light. Lu et al. [31] created p-n heterojunctions of TiO_2 modified with flower-like and bulk-like $Co(OH)_2$ using a solvothermal method. Varied morphologies led to distinctions in the photo-electro-chemical performance. As indicated by the experimental findings, TiO_2 modified with flower-like $Co(OH)_2$ microspheres exhibited a narrower bandgap, an upward shift in the CB, and a more rapid separation and migration of carriers compared to bulk-like $Co(OH)_2$. Moreover, the TiO_2 photoelectrode modified with flower-like $Co(OH)_2$ microspheres exhibited a relatively low photo-potential of −0.53 V in a 3.5 wt% NaCl solution, thereby offering effective PCP for 304 SS. Zhang et al. [32] synthesized a composite photoanode of CdSe/CdS/PbS/TiO_2 using the successive ionic layer adsorption (SILAR) method, achieving a solar energy conversion rate of 5.11%. Gong et al. [33] deposited ZnSe onto the surface of TiO_2 nanorods by electrodeposition to obtain TiO_2/ZnSe composites (Figure 3A), and systematically investigated the effects of Na_2S, Na_2SO_4, Na_2SO_3, $Na_2S_2O_3$ and NaCl as sacrificial reagents on the protection of 304 SS by TiO_2/ZnSe composites. The migration and consumption of photogenerated holes at the photoanode were governed by the redox potential of the sacrificial reagents (Figure 3B). As shown in Figure 3C, the most negative redox potential of TiO_2/ZnSe photoanode was in the Na_2S medium.

Table 2. Comparison of PCP performances of semiconductor composite TiO_2 materials.

Samples	Electrochemical Cell Medium	Metal	Potential Drop/mV	Reference
SnO_2/TiO_2	3.5 wt% NaCl	304 SS	240	[25]
g-$C_3N_4/SrTiO_3/TiO_2$	0.5 M KOH solution	403 SS	680	[26]
$In_2S_3/Ag_2S/TiO_2$	3.5 wt% NaCl	Q235 CS	340	[27]
NiO/TiO_2	0.5 M KOH and 1 M CH_3OH mixed solution	403 SS	340	[28]
Ag/SnO_2/TiO_2	0.2 M KOH aqueous solution with 20 vol% ethylene glycol	403 SS	475	[29]
MoS_2/TiO_2	0.25 M Na_2S and 0.35 M Na_2SO_3 solution	304 SS	360	[30]

Three-component metal sulfides possess unique optoelectronic properties and stability, with a narrow bandgap and a more negative conduction band potential. This enables them to broaden the visible light response range and boost the density of charge carriers in TiO_2, thereby facilitating the separation of photo-generated electron-hole pairs and providing protection to metals with more negative self-corrosion potentials. Ma et al. [34] successfully prepared $TiO_2/ln_2S_3/AgInS_2$ by two-step anodization of titanium foil followed by ion layer adsorption and reaction. $TiO_2/ln_2S_3/AgInS_2$ exhibited high photocatalytic activity under visible light, with a significant decrease in the photocurrent potential of up to 950 mV and a

decrease in current density of up to 30 A·cm^{-2}. Therefore, compared to pure TiO_2, coupled with 304 SS, $TiO_2/ln_2S_3/AgInS_2$ can provide more efficient photo-electro-chemical cathodic protection under visible light. Sun et al. [35] also prepared and optimized $AgInS_2/In_2S_3$ nanoparticles co-sensitized TiO_2 nanotube array photoanodes with an In_2S_3 buffer layer around the $AgInS_2$ absorber layer (Figure 4). The In_2S_3 buffer layer around the absorber layer greatly enhances the efficiency of charge generation and separation in the prepared photoanodes. Li et al. [36] successfully prepared $ZnIn_2S_4/TiO_2$ nanotube composites by combining hydrothermal reaction with electrochemical anodic oxidation. The photo-electric current density of the 3D $ZnIn_2S_4/TiO_2$ nanotube composites coupled with Q235 carbon steel (CS) can reach 400 mA/cm^2, and the composite photoanode exhibits a photo-generated potential drop of approximately 360 mV, providing an effective PCP for Q235 CS under visible light irradiation. Li et al. [37] successfully prepared $SnIn_4S_8/TiO_2$ composites through solvent-thermal treatment and electrochemical anodic oxidation. $SnIn_4S_8$ has a large specific surface area and its nanosheets have relatively negative conduction bands, therefore, $SnIn_4S_8$ nanosheets modified TiO_2 had better photo-electro-chemical and PCP properties. Additionally, the maximum photo-electric current density of the composite material during a 6 h solvent-thermal reaction under visible light irradiation is 100 μA cm^{-2}, and the negative shift of the photo-induced potential for Q235 CS connected to the composite material can reach −450 mV. In addition, many other three-component metal sulfides are used to complex TiO_2 and to modify the PCP effect of TiO_2 on metals [38–41].

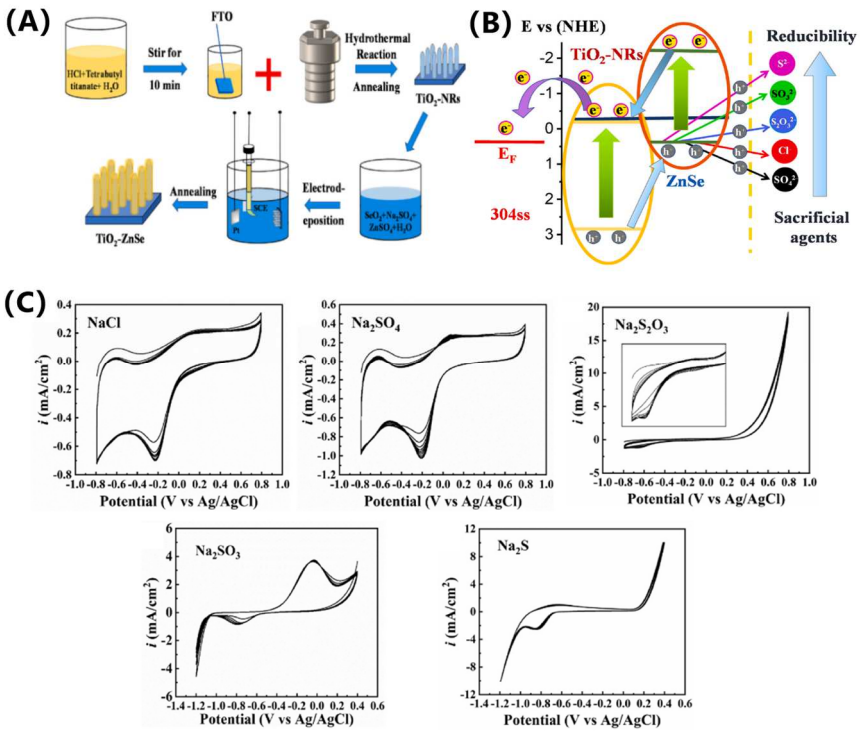

Figure 3. (**A**) Preparation process of TiO_2 and TiO_2/ZnSe film; (**B**) Cyclic voltammetry curve of NaCl, Na_2SO_4, $Na_2S_2O_3$, Na_2SO_3, Na_2S; (**C**) PCP mechanism of TiO_2/ZnSe under illumination [33].

Graphene is a zero-bandgap material with excellent electronic transport properties, ample specific surface area, and robust chemical stability [42], which can enhance the photo-electro-chemical protection effect of TiO_2. Shen et al. [43] prepared CdSe/rGO/TiO_2 composite films using a two-step electrodeposition method and an anodic oxidation method. The composite film consists of uniform rutile TiO_2 nanotube arrays, graphene sheets, and cubic CdSe nanoparticles, exhibiting high light absorption in the UV and visible light regions. The visible light-induced photocurrent can achieve a level of approximately 750 μA/cm^2, achieving effective charge separation. Li et al. [44] employed cyclic voltammetry deposition to coat the surface of TiO_2 nanotubes with graphene and CdTe nanoparticles,

forming CdTe/graphene/TiO_2 composite materials. Graphene functions as a mediator in electron transfer, while CdTe acts as a visible light sensitizer. The introduction of graphene between CdTe and TiO_2 interfaces enhances charge separation, accelerates carrier transfer, and reduces charge recombination. Under visible light irradiation, the potential of the SS coupled with CdTe/graphene/TiO_2 quickly decreases to −750 mV, lower than the initial potential of SS (−180 mV). After turning off the light source, pure TiO_2 fails to maintain its protective effect, while the composite film exhibits a delay in the cathodic protection time of SS of more than 8 h, indicating a significant delayed protection effect and excellent PCP of 304 SS. Li et al. [45] prepared $ZnIn_2S_4$/rGO/TiO_2 nanotube photoanodes by combining electrochemical anodization and hydrothermal methods. The bandgap difference between $ZnIn_2S_4$ and rGO contributes to the establishment of a heterojunction electric field with TiO_2 facilitating efficient charge separation and transfer, and greatly improving the photo-electro-chemical activity of the composite material. Li et al. [46] synthesized TiO_2 nanocomposites co-sensitized with $AgInS_2$ and graphene through a combination of hydrothermal reaction and electrochemical anodization. The photo-induced potential reduction of $AgInS_2$/graphene/TiO_2 composite material can achieve 680 mV. The Tafel curve results suggest that the incorporation of graphene enhances the photo-electro-catalytic protection effect of $AgInS_2$/TiO_2. Experimental results demonstrate that $AgInS_2$/graphene/TiO_2 composite material exhibits good PCP performance.

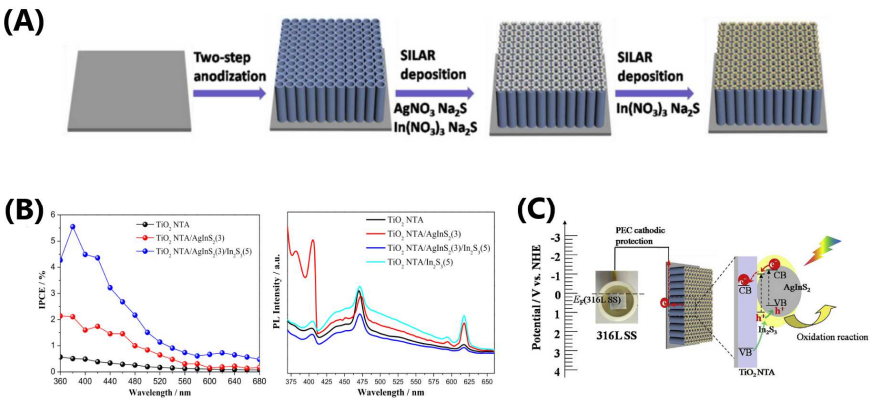

Figure 4. (**A**) Fabrication process of TiO_2/$AgInS_2$/In_2S_3; (**B**) IPCE and photoluminescence spectra of different TiO_2 photoanodes; (**C**) PCP mechanism of TiO_2 NTA/$AgInS_2$(3)/In_2S_3(5) under visible light [35].

2.3. Energy Storage Materials

SnO_2 is an n-type semiconductor with photo-electro-chemical performance akin to TiO_2. In addition, its electron mobility is higher than that of TiO_2, both in single crystals and the corresponding nanostructures, which makes SnO_2 ideal for high-performance optoelectronic devices. Literature has shown that SnO_2 is often used as an energy storage material. Hu et al. [47] prepared tetragonal SnO_2 films on FTO conductive glass by pulsed current deposition, and the results showed that the SnO_2 films were photoreactive, and the annealed films were more stable under prolonged illumination. The results showed that the SnO_2 film was photoactive, the annealed film was more stable under prolonged light exposure, and it could effectively protect 403 SS under light exposure in 0.5 mol/L NaCl solution, and the galvanic coupling effect after the light was turned off had a corrosion protection effect on SS. Zhu et al. [48] synthesized $ZnIn_2S_4$/SnO_2/TiO_2 composites, comprising $ZnIn_2S_4$ nanosheets and SnO_2 quantum dots co-modified with TiO_2 nanotubes. This was achieved through anodic oxidation, in-situ impregnation, and hydrothermal methods (Figure 5). It was found that the photocurrent density of the $ZnIn_2S_4$/SnO_2/TiO_2 composites under visible light was as high as 715 μA cm^{-2}, which was 25 times higher than that of pure TiO_2. This improvement is primarily attributed to $ZnIn_2S_4$ nanosheets to extend the light absorption into the visible spectrum. In addition, the SnO_2 quantum dots enhanced the energy storage efficiency of the composite, allowing the composite to offer

delayed protection for the protected metal for up to 10 h in the absence of light. In addition, they found that the heterojunction structure formed between TiO_2, SnO_2, and $CaIn_2S_4$ could promote the separation and transfer efficiency of electrons and holes (Figure 6). The presence of SnO_2 nanoflowers gave the $CaIn_2S_4/SnO_2/TiO_2$ composites an outstanding electron storage capacity, which allowed them to provide time-delayed protection of Q235 carbon steel for up to 10 h in the absence of light [49].

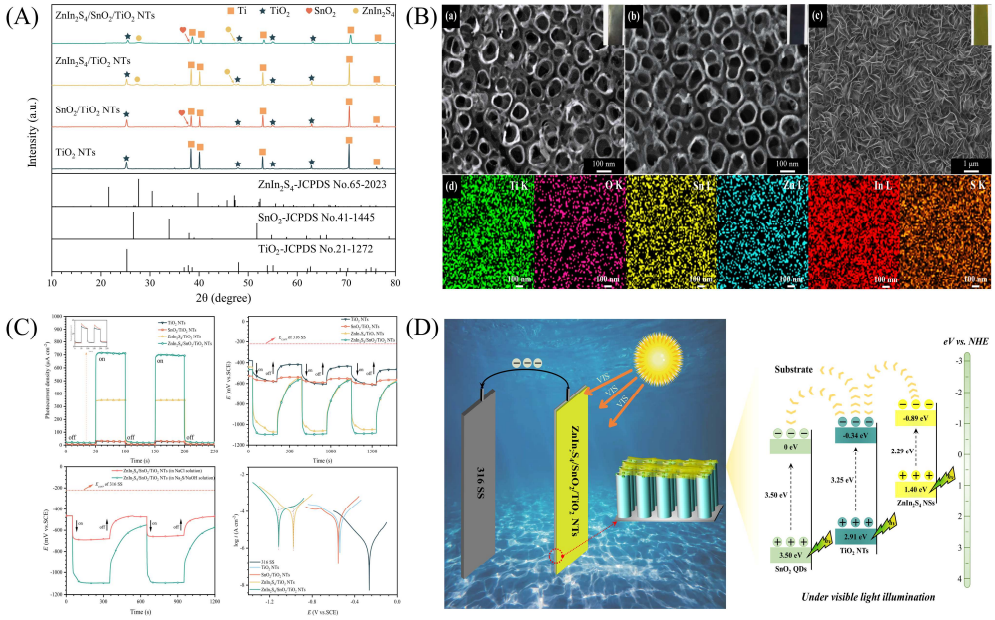

Figure 5. (**A**) XRD patterns of $ZnIn_2S_4/SnO_2/TiO_2$; (**B**) SEM and EDS images; (**C**) Photocurrent variation curves, Open-circuit potential variation curves, and polarization curves of 316 SS coupled with different photoanodes under open and closed light conditions; (**D**) Protection mechanism [48].

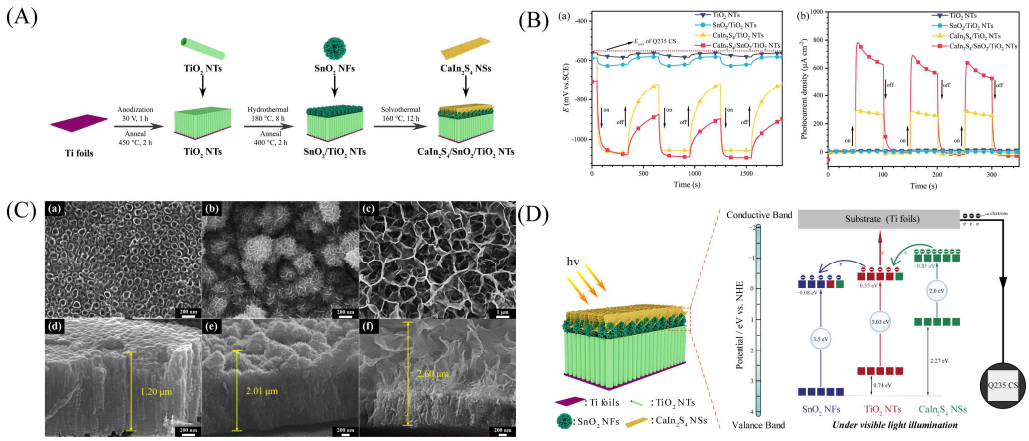

Figure 6. (**A**) Flowchart of the preparation of $CaIn_2S_4/SnO_2/TiO_2$; (**B**) SEM images; (**C**) Variation curves of the photoluminescent current and photo-open potential of Q235 carbon steel coupled with different photoanodes under open and closed light conditions; (**D**) Protection mechanism diagram [49].

Tungsten trioxide (WO_3) is considered as a potential material for photoelectrodes due to its wide range of photo-responses, high electron mobility, and non-toxicity. The process of storing electrons and releasing electrons from WO_3 is realized by the conversion between $MxWO_3$ (M = H, Li, Na, etc.) and WO_3. Under light, WO_3 store electrons in the form of $MxWO_3$. Under dark conditions, the stored electrons are released and $MxWO_3$ is converted to WO_3, which enables continuous PCP of coupled metallic materials [50,51].

However, WO_3 semiconductors suffer from the drawbacks of low efficiency of photo-generated electron-hole separation and inability to charge themselves. Tian et al. [52] constructed $WO_3/ZnIn_2S_4$ composites with good dark continuous PCP performance by utilizing $ZnIn_2S_4$-modified WO_3, which has a more negative CB potential. Its photo-generated potential drop in NaCl solution can reach 332.8 mV, which is markedly superior to that of WO_3 and $ZnIn_2S_4$ photoelectrodes. Meanwhile, the $ZnIn_2S_4$ composite on WO_3 can charge WO_3 under light, allowing the $WO_3/ZnIn_2S_4$ photoanode to continue providing protection for the coupled 304 SS even after the light is turned off. The $WO_3/ZnIn_2S_4$ heterojunction photoelectrode can store 0.17 C electrons when the light illumination time is 2 h, which can offer protection for the coupled 304 SS in the dark state for 11.88 h after the light is turned off. Zhu et al. [53] successfully prepared $CdIn_2S_4/WO_3/TiO_2$ photoanodes by using anodic oxidation and a two-step hydrothermal method to deposit WO_3 nanosheets and $CdIn_2S_4$ nanoparticles sequentially on TiO_2 nanotubes (Figure 7). The researchers explored the effects of different hydrothermal times on the PCP performance of the prepared photoanodes, and the best PCP performance of $CdIn_2S_4/WO_3/TiO_2$ on Q235 carbon steel was achieved when the hydrothermal time of both steps was 6 h. The PCP of Q235 carbon steel was achieved with the highest photocurrent density (633 μA cm^{-2}), the lowest charge transfer resistance (11.34 Ω·cm^2), and the largest open-circuit potential drop (490 mV vs. SCE). The researchers analyzed the work function of $CdIn_2S_4$, WO_3, TiO_2, and $CdIn_2S_4/WO_3/TiO_2$ by DFT calculations. In addition, $CdIn_2S_4/WO_3/TiO_2$ can provide continuous protection for Q235 carbon steel in the dark for up to 10 h.

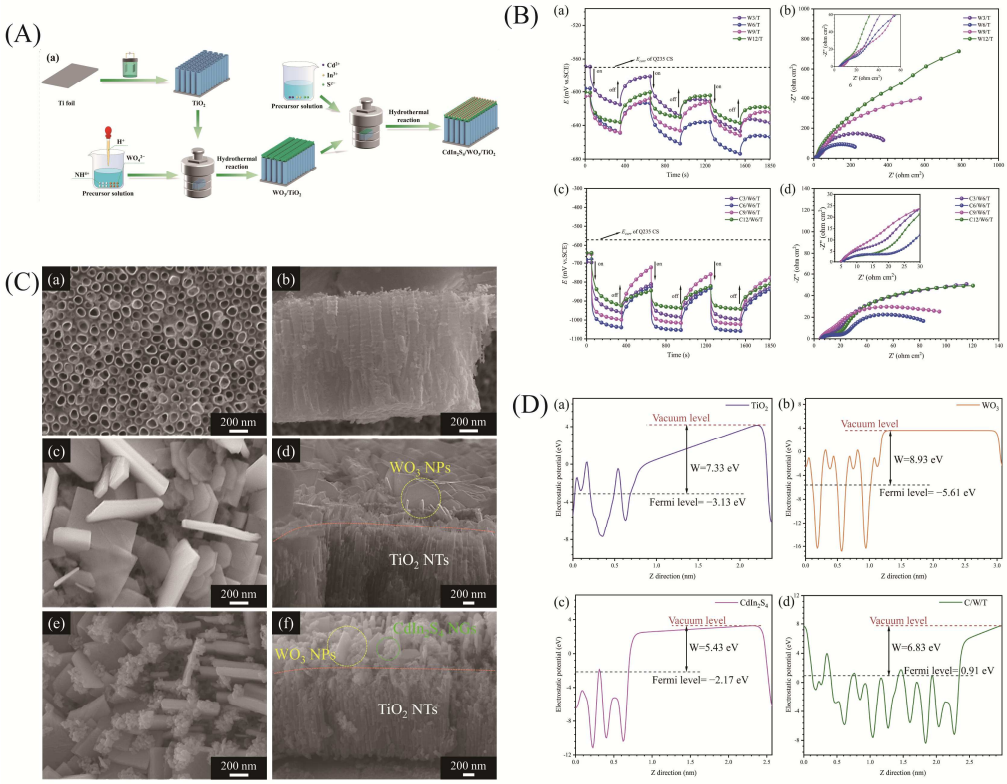

Figure 7. (**A**) Flow chart of the preparation of $CdIn_2S_4/WO_3/TiO_2$; (**B**) SEM images; (**C**) Photo-open potential change curves and electrochemical impedance spectra of Q235 carbon steel coupled with photoanodes of different hydrothermal times under open and closed light conditions; (**D**) DFT calculations [53].

3. Common New Photoanode Materials

With the in-depth study of photogenerated cathode protection systems, some new non-TiO_2-based photoelectrodes have also attracted wide attention, and several new photoelectrodes are briefly introduced in the following.

$BiVO_4$ is an n-type semiconductor, which is a very promising photo-anode material due to its narrow band gap (~2.4 eV) structure, easy preparation, and appropriate band-edge position [54]. However, its PCP performance is affected by the low charge separation and transfer efficiency, so it is necessary to develop efficient $BiVO_4$-based systems to enhance its PCP performance. Li et al. [55] achieved long-term protection of 304 SS under simulated solar irradiation by modifying $BiVO_4$ films using CoFe Prussian Blue (CoFe-PB) electrocatalyst. The aligned energy band configuration facilitated the efficient transfer of holes from the $BiVO_4$ valence band to CoFe-PB, enabling the swift injection of CoFe-PB holes into the electrolyte solution. This significantly reduces electron-hole recombination and enhances the transfer of electrons from the $BiVO_4$ photoelectrode to the 304 SS after irradiation. Yang et al. [56] prepared direct Z-type nanoporous CdS by using the electrodeposition and SILAR methods quantum dots/$BiVO_4$ heterojunction photoelectrodes by electrodeposition and SILAR. The incorporation of CdS quantum dots markedly enhanced the efficiency of visible light utilization in the composites. The CdS(8)/$BiVO_4$ prepared after 8 SILAR processes showed the best PCP performance on 316 SS in 3.5 wt% NaCl solution. As shown in Figure 8, the Z-type heterojunction carrier transfer mechanism is conformed between CdS and $BiVO_4$, and the holes and electrons are effectively separated spatially, which enhances the protective effect of $BiVO_4$ on 316 SS. Additionally, they achieved the successful synthesis of polyhedral ZIF-67 on the $BiVO_4$ substrate through electrodeposition and in-situ growth [57]. It was found that the ZIF-67/$BiVO_4$ heterojunction photoanode without a hole scavenger showed excellent PCP properties against 316 SS under visible light irradiation. The OCP drop of ZIF-67-150s/$BiVO_4$ coupled 316 SS was 240 mV more than that of $BiVO_4$. The in-situ grown ZIF-67 formed a tight connection with $BiVO_4$, thereby significantly enhancing charge transfer efficiency. The expansive specific surface area and the microporous/mesoporous structure of ZIF-67/$BiVO_4$ also improve the interaction between the active sites and the electrolyte, which facilitated the carrier migration in the electrolyte. In addition, the reduction of the composite work function promotes the electron transfer to 316 SS. Chen et al. [58] prepared WO_3@$BiVO_4$ nanospherical composites using a hydrothermal method. The electrochemical tests, such as polarization curves, impedance tests, and open-circuit potentials, illustrated that the WO_3@$BiVO_4$ composites not only effectively pulled down the inherent corrosion potential of 304 SS, but also that the introduction of WO_3 enhanced the electron-hole separation efficiency of $BiVO_4$, showed good energy storage capacity, and effectively improved the PCP performance of $BiVO_4$. Guo et al. [59] prepared WO_3/$BiVO_4$ composite films by spin coating and hydrothermal method, and some $BiVO_4$ particles were converted to Bi_2S_3 particles in situ in electrochemical tests under light. This special ternary heterojunction structure not only can effectively reduce the corrosion potential of 304 SS, but also the in situ generated Bi_2S_3 can effectively inhibit the carrier recombination of $BiVO_4$, and can enhance the response of WO_3/$BiVO_4$ material to visible light, which effectively improves the PCP performance of $BiVO_4$.

g-C_3N_4 is a typical polymer semiconductor (~2.7 eV), which has garnered significant attention because of its easy synthesis and suitable energy band structure, excellent optical properties, and high physicochemical stability, but its photogenerated carriers are easy to be recombined limiting its further application [60–62]. Zheng et al. [63] synthesized a two-step hydrothermal method to synthesize g-C_3N_4/rGO/ZnS composites, and the results showed that the PCP performance of the ternary composites on 304 SS was improved compared with that of pure g-C_3N_4. Especially noteworthy is the coupling of 304 SS with 15% rGO/g-C_3N_4/ZnS composites, resulting in a photocurrent density of 2180 $\mu A/cm^2$ at a bias of -0.23 V (vs. SCE). This value is approximately four times greater than that achieved with pure g-C_3N_4. The increased PCP performance for 304 SS is credited to the significantly high efficiency in the separation of charge carriers.

ZnO is an n-type semiconductor with excellent photo-electro-chemical activity, controllable microstructure, easy to make nanorods, nanoribbons, and nanowires, and low toxicity, and abundant raw material advantages [64–66]. Yang et al. [67] fabricated Co_3O_4@ZnO and found that PCP enhancement is ascribed to the narrow band gap of Co_3O_4 and the

formation of a p-n junction at the Co_3O_4/ZnO interface. The photocurrent density of the Co_3O_4@ZnO nanocomposite photoelectrode connected to 304 SS under visible light reached 10.5 μA/cm^2 with a cathodic polarization potential of −720 mV (vs. SCE).

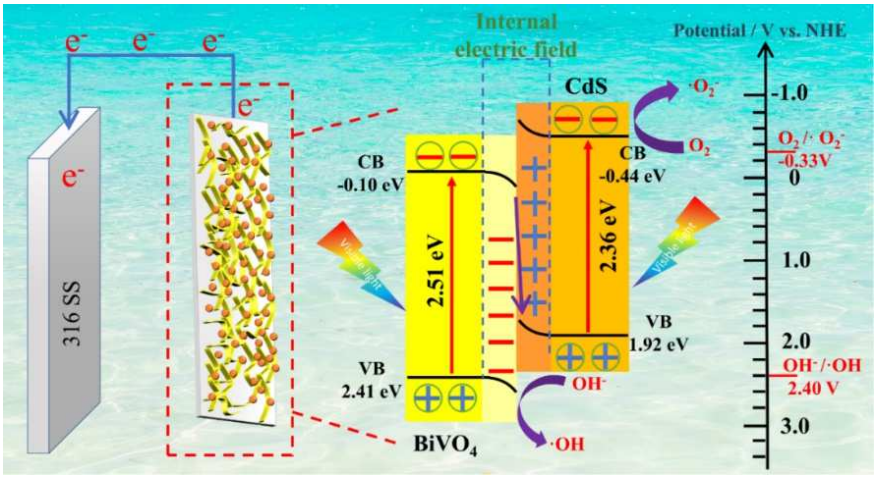

Figure 8. Carrier migration mechanism of CdS/$BiVO_4$ heterojunction [56].

The band gap energy of In_2O_3 is approximately ~2.8 eV, and the CB potential is more negative than the self-corrosion potential of metals [68]. Therefore, In_2O_3 thin film is a potential corrosion-resistant photoanode. Zhang et al. [69] synthesized In_2O_3 powder by sol-gel and solid-phase methods and studied its photo-electro-chemical behavior under visible light irradiation. The relatively small particle size of the In_2O_3 powder prepared using the sol-gel method facilitates the transfer of electrons, which improves the performance of PCP for 304 SS under visible light irradiation.

The band gaps of $SrTiO_3$ and TiO_2 are similar (~3.2 eV), but the conduction band edge of $SrTiO_3$ is 200 mV less than that of TiO_2, which suggests that $SrTiO_3$ is more likely to polarize the metal [70–72]. Yang et al. [73] synthesized a bilayered CeO_2/$SrTiO_3$ nanocomposite photoelectrode through the sol-gel and microemulsion methods, and the photoelectrode could be used for the cathodic polarization of 304 SS in a 3.5% (mass fraction) NaCl solution for photogenerated cathodic protection under light. Because of the photoelectron generation from the external $SrTiO_3$ layer, the prepared photoelectrode can be catholically polarized on 304 SS in 3.5% (mass fraction) NaCl solution, and photo-generated cathodic protection was carried out in the presence of light. In the absence of light, the photoelectrodes can sustain their corrosion protection by transferring the charge stored in the CeO_2 layer to the steel, providing protection to the steel even in the absence of light.

4. Conclusions

Since clean solar energy can be utilized and the photoanode material does not need to be consumed, PCP technology has garnered significant attention from scholars both domestically and internationally. TiO_2 has been widely studied because of its low toxicity, simple preparation, and high stability. However, its low utilization of sunlight and high photogenerated carrier complex rate severely limit its application in PCP. This study describes the modification of TiO_2 to improve the PCP performance using metal and non-metal doping, Semiconductor compounding, and shape control. (1) The use of special ordered nanostructures can not only effectively shorten the photocarrier transport distance of semiconductor materials, but also enhance the active site of photo-electro-chemical reaction. (2) Elemental doping not only introduces impurity energy levels and reduces the band gap in semiconductor materials to improve their optical absorption capacity, but also increases the carrier concentration of semiconductor materials, thereby improving the photogenerated charge transfer rate. However, elemental doping methods are effective for protecting stainless steel, but not sufficient for protecting metals with negative self-

corrosion potentials. (3) The construction of a heterojunction structure can effectively expand the spectrum of light absorption and promote carrier separation and transfer by attaching a semiconductor with a narrow bandgap to the main semiconductor. In particular, semiconductors with negative conduction band potentials, such as ternary sulfide materials, which have good optoelectronic properties and stability, can provide protection for metals with negative self-corrosion potentials. In addition, graphene has excellent electron transport properties, sufficient specific surface area, and strong chemical stability, and can be used as an effective electron carrier. (4) Combining semiconductor materials with a high electron storage capacity (WO_3 or SnO_2) allows for continuous protection of the metal after the light is cut off. These strategies on the modification of semiconductor materials are important for improving the performance of PCP. This paper also reviews other novel semiconductor photoanodes such as $BiVO_4$, g-C_3N_4, ZnO, In_2O_3, and $SrTiO_3$.

Although much progress has been made in the development and research of semiconductor materials for PCP, there are still several issues that need to be resolved to realize the practical applications of PCP: (1) Most of the electrolytes in the PCP process contain hole scavengers that promote pair carrier separation, so there is a need to develop materials that will work in real marine environments. (2) Design and development of Z-scheme heterojunction composite photoanodes for improved redox capability that can drive more electrons for cathodic protection of a wider variety of metals. (3) There is an urgent need to develop more effective means of studying the mechanisms of the charge transfer process during PCP. In situ transient absorption spectroscopy methods and density-functional theory (DFT) calculations can be used to study the photo-generated charge transfer process and provide a theoretical foundation for the precise design of semiconductor functional materials for efficient PCP.

Author Contributions: Picture drawing, Writing—original draft, review & editing, M.Y.; Data Curation, R.J.; Writing—review & editing, J.Z.; Writing—review & editing, X.Z.; Writing—review & editing, G.L.; Writing—review & editing, W.L.; Resources, F.M.; Writing—review & editing, X.J.; Resources, Funding acquisition, Writing—review & editing, H.L. All authors have read and agreed to the published version of the manuscript.

Funding: This work was funded by the Natural Science Foundation of Shandong Province of China (No. ZR2023ME205), and the National Natural Science Foundation of China (No. 51801109).

Institutional Review Board Statement: Not applicable.

Informed Consent Statement: Not applicable.

Data Availability Statement: The authors confirm that the data supporting the findings of this study are available within the article.

Conflicts of Interest: The authors declare no conflicts of interest.

References

1. Tang, J.; Yang, M.Y.; Kainuma, S. Electrochemical interaction behaviours between adjacent coating defects in steel structure associated with corrosion acceleration effects. *Corros. Sci.* **2024**, *227*, 112694. [CrossRef]
2. Tian, Y.; Zhang, G.Y.; Ye, H.L.; Zeng, Q.; Zhang, Z.D.; Tian, Z.S.; Jin, X.Y.; Jin, N.G.; Chen, Z.G.; Wang, J.X. Corrosion of steel rebar in concrete induced by chloride ions under natural environments. *Constr. Build. Mater.* **2023**, *369*, 130504. [CrossRef]
3. Liao, B.K.; Ma, S.Q.; Zhang, S.Y.; Li, X.X.; Quan, R.X.; Wan, S.; Guo, X.P. Fructus cannabis protein extract powder as a green and high effective corrosion inhibitor for Q235 carbon steel in 1 M HCl solution. *Int. J. Biol. Macromol.* **2023**, *239*, 124358. [CrossRef] [PubMed]
4. Yu, K.D.; Zhao, W.; Li, Z.; Guo, N.; Xiao, G.C.; Zhang, H. High-temperature oxidation behavior and corrosion resistance of in-situ TiC and Mo reinforced AlCoCrFeNi-based high entropy alloy coatings by laser cladding. *Ceram. Int.* **2023**, *49*, 10151–10164. [CrossRef]
5. Xu, W.; Chen, Y.L.; Chen, L.Q.; Huang, H.; Li, C.C. Effect of cathodic protection potential change caused by alternating current interference on corrosion behavior of X90 steel in 3% NaCl solution. *Int. J. Electrochem. Sci.* **2022**, *17*, 221019. [CrossRef]

6. Liu, Y.P.; Wang, Z.Y.; Lin, C.Z.; Zhang, J.T.; Feng, J.T.; Hou, B.; Yan, W.; Li, M.T.; Ren, Z.J. Spontaneous polarization of ferroelectric heterostructured nanorod arrays for high-performance photoelectrochemical cathodic protection. *Appl. Surf. Sci.* **2023**, *609*, 155345. [CrossRef]
7. Yun, T.H.; Kim, T.; Kim, M.T.; Park, J.H.; Kim, S.J. Enhancing corrosion resistance of carbon steel and stainless steel through photocathodic protection using TiO_2-polyvinyl butyral electrophoretic deposition coating. *J. Ind. Eng. Chem.* **2023**, *126*, 408–417. [CrossRef]
8. Chen, X.; Zhou, G.Z.; Wang, X.T.; Xu, H.; Wang, C.Z.; Yao, Q.H.; Chi, J.Y.; Fu, X.N.; Wang, Y.H.; Yin, X.Y.; et al. Progress in semiconductor materials for photocathodic protection: Design strategies and applications in marine corrosion protection. *Chemosphere* **2023**, *323*, 138194. [CrossRef]
9. Cui, J.; Pei, Y.S. Enhanced photocathodic protection performance of Fe_2O_3/TiO_2 heterojunction for carbon steel under simulated solar light. *J. Alloys Compd.* **2019**, *779*, 183–192. [CrossRef]
10. Guo, H.X.; Li, L.L.; Su, C.; Yu, D.M.; Liu, Z.Y. Effective photocathodic protection for 304 stainless steel by PbS quantum dots modified TiO_2 nanotubes. *Mater. Chem. Phys.* **2021**, *258*, 123914. [CrossRef]
11. Yang, Y.; Cheng, Y.F. Visible light illuminated high-performance WO_3-TiO_2-$BiVO_4$ nanocomposite photoanodes capable of energy self-storage for photo-induced cathodic protection. *Corros. Sci.* **2020**, *164*, 108333. [CrossRef]
12. Li, W.F.; Wei, L.C.; Shen, T.; Wei, Y.N.; Li, K.J.; Liu, F.Q.; Li, W.H. Ingenious preparation of "layered-closed" TiO_2-$BiVO_4$-CdS film and its highly stable and sensitive photoelectrochemical cathodic protection performance. *Chem. Eng. J.* **2022**, *429*, 132511. [CrossRef]
13. Liu, Y.; Xu, C.; Feng, Z.D. Characteristics and anticorrosion performance of Fe-doped TiO_2 films by liquid phase deposition method. *Appl. Surf. Sci.* **2014**, *314*, 392–399. [CrossRef]
14. Eshaghzadeh, F.; Momeni, M.M.; Farrokhpour, H. Preparation of Iron and Chromium Co-Doped TiO_2 Nanotubes and Study of Their Photoelectrochemical Properties. *J. Electron. Mater.* **2023**, *52*, 6977–6991. [CrossRef]
15. Sun, M.M.; Chen, Z.Y.; Yu, J.Q. Highly efficient visible light induced photoelectrochemical anticorrosion for 304 SS by Ni-doped TiO_2. *Electrochim. Acta* **2013**, *109*, 13–19. [CrossRef]
16. Momeni, M.M.; Khansari-Zadeh, S.H.; Farrokhpour, H. Fabrication of tungsten-iron-doped TiO_2 nanotubes via anodization: New photoelectrodes for photoelectrochemical cathodic protection under visible light. *SN Appl. Sci.* **2019**, *1*, 1160. [CrossRef]
17. Momeni, M.M.; Motalebian, M.; Ghayeb, Y.; Atapour, M. Photoelectrochemical Cathodic Protection of Stainless Steel using W- and Cr-Doped/Codoped TiO_2 Nanotube Thin Film Photoanodes. *J. Electrochem. Soc.* **2021**, *168*, 081504. [CrossRef]
18. Li, J.; Lin, C.J.; Lai, Y.K.; Du, R.G. Photogenerated cathodic protection of flower-like, nanostructured, N-doped TiO_2 film on stainless steel. *Surf. Coat. Technol.* **2010**, *205*, 557–564. [CrossRef]
19. Yin, J.K.; Lv, L.L.; Chu, Y.Q.; Tan, L.J. Highly antibacterial Cu/Fe/N co-doped TiO_2 nanopowder under visible light. *Inorg. Chem. Commun.* **2023**, *151*, 110587. [CrossRef]
20. Zhu, L.; Cui, X.L.; Shen, J.; Yang, X.L.; Zhang, Z.J. Visible light photoelectrochemical response of carbon-doped TiO_2 thin films prepared by DC reactive magnetron sputtering. *Acta Phys. Chim. Sin.* **2007**, *23*, 1662–1666. [CrossRef]
21. Lei, C.X.; Feng, Z.D.; Zhou, H. Visible-light-driven photogenerated cathodic protection of stainless steel by liquid-phase-deposited TiO_2 films. *Electrochim. Acta* **2012**, *68*, 134–140. [CrossRef]
22. Arman, S.Y.; Omidvar, H.; Tabaian, S.H.; Sajjadnejad, M.; Fouladvand, S.; Afshar, S. Evaluation of nanostructured S-doped TiO_2 thin films and their photoelectrochemical application as photoanode for corrosion protection of 304 stainless steel. *Surf. Coat. Technol.* **2014**, *251*, 162–169. [CrossRef]
23. Momeni, M.M.; Taghinejad, M.; Ghayeb, Y.; Bagheri, R.; Song, Z. Preparation of various boron-doped TiO_2 nanostructures by in situ anodizing method and investigation of their photoelectrochemical and photocathodic protection properties. *J. Iran. Chem. Soc.* **2019**, *16*, 1839–1851. [CrossRef]
24. Jiang, X.H.; Sun, M.M.; Chen, Z.Y.; Jing, J.P.; Feng, C. High-efficiency photoelectrochemical cathodic protection performance of the $TiO_2/AgInSe_2/In_2Se_3$ multijunction nanosheet array. *Corros. Sci.* **2020**, *176*, 108901. [CrossRef]
25. Zhang, J.T.; Yang, H.L.; Wang, Y.; Cui, X.H.; Wen, Z.; Liu, Y.P.; Fan, L.; Feng, J.T. Facile fabrication of SnO_2 modified TiO_2 nanorods film for efficient photocathodic protection of 304 stainless steel under simulated solar light. *Corros. Sci.* **2020**, *176*, 108927. [CrossRef]
26. Guan, Z.C.; Hu, J.; Wang, H.H.; Shi, H.Y.; Wang, H.P.; Wang, X.; Jin, P.; Song, G.L.; Du, R.G. Decoration of rutile TiO_2 nanorod film with g-$C_3N_4/SrTiO_3$ for efficient photoelectrochemical cathodic protection. *J. Photochem. Photobiol. A* **2023**, *443*, 114825. [CrossRef]
27. Li, H.; Yang, Z.Y.; Cui, X.Q.; Li, Y.H.; Zhang, P.F.; Li, J.R. A highly efficient $In_2S_3/Ag_2S/TiO_2$ NTAs photoelectrodes for photocathodic protection of Q235 carbon steel under visible light. *Nanotechnology* **2023**, *34*, 045705. [CrossRef]
28. Jin, P.; Guan, Z.C.; Liang, Y.; Tan, K.; Wang, X.; Song, G.L.; Du, R.G. Photocathodic Protection on Stainless Steel by Heterostructured NiO/TiO_2 Nanotube Array Film with Charge Storage Capability. *Acta Phys. Chim. Sin.* **2021**, *37*, 1906033. [CrossRef]
29. Wang, H.P.; Guan, Z.C.; Shi, H.Y.; Wang, X.; Jin, P.A.; Song, G.L.; Du, R.G. $Ag/SnO_2/TiO_2$ nanotube composite film used in photocathodic protection for stainless steel. *J. Photochem. Photobiol. A* **2021**, *417*, 113353. [CrossRef]
30. Ma, X.M.; Ma, Z.; Lu, D.Z.; Jiang, Q.T.; Li, L.L.; Liao, T.; Hou, B.R. Enhanced photoelectrochemical cathodic protection performance of MoS_2/TiO_2 nanocomposites for 304 stainless steel under visible light. *J. Mater. Sci. Technol.* **2021**, *64*, 21–28. [CrossRef]

31. Lu, X.Y.; Liu, L.; Xie, X.; Cui, Y.; Oguzie, E.E.; Wang, F.H. Synergetic effect of graphene and $Co(OH)_2$ as cocatalysts of TiO_2 nanotubes for enhanced photogenerated cathodic protection. *J. Mater. Sci. Technol.* **2020**, *37*, 55–63. [CrossRef]
32. Zhang, X.L.; Lin, Y.; Wu, J.H.; Jing, J.; Fang, B.P. Improved performance of CdSe/CdS/PbS co-sensitized solar cell with double-layered TiO_2 films as photoanode. *Opt. Commun.* **2017**, *395*, 117–121. [CrossRef]
33. Gong, D.M.; Xu, S.W.; Zhang, K.L.; Du, L.L.; Qiu, P. Enhancing photoelectrochemical cathodic protection performance by facile tuning sulfur redox state in sacrificial agents. *Chem. Eng. J.* **2023**, *451*, 138552. [CrossRef]
34. Ma, X.M.; Ma, Z.; Lu, D.Z.; Li, L.L.; Liao, T.; Hou, B.R. Preparation of $In_2S_3/AgInS_2/TiO_2$ nanotube arrays and enhanced photoelectrochemical cathodic protection for 304 SS under visible light. *J. Photochem. Photobiol. A* **2022**, *433*, 114143. [CrossRef]
35. Sun, M.M.; Chen, Z.Y.; Li, J.R.; Hou, J.; Xu, F.L.; Xu, L.K.; Zeng, R.C. Enhanced visible light-driven activity of TiO_2 nanotube array photoanode co-sensitized by "green" $AgInS_2$ photosensitizer and In_2S_3 buffer layer. *Electrochim. Acta* **2018**, *269*, 429–440. [CrossRef]
36. Li, H.; Li, Y.H.; Wang, X.T.; Hou, B.R. 3D $ZnIn_2S_4$ nanosheets/TiO_2 nanotubes as photoanodes for photocathodic protection of Q235 CS with high efficiency under visible light. *J. Alloys Compd.* **2019**, *771*, 892–899. [CrossRef]
37. Li, H.; Song, W.Z.; Cui, X.Q.; Li, Y.H.; Hou, B.R.; Cheng, L.J.; Zhang, P.F. Preparation of $SnIn_4S_8/TiO_2$ Nanotube Photoanode and Its Photocathodic Protection for Q235 Carbon Steel Under Visible Light. *Nanoscale Res. Lett.* **2021**, *16*, 10. [CrossRef] [PubMed]
38. Liu, J.; Wang, N.; Zheng, F.W.; Wang, C.X.; Wang, J.; Hou, B.R.; Zhao, Q.Y.; Ning, Y.L.; Hu, Y.T. $CuInS_2/TiO_2$ heterojunction with elevated photo-electrochemical performance for cathodic protection. *J. Mater. Sci. Technol.* **2022**, *122*, 211–218. [CrossRef]
39. Jiang, X.H.; Sun, M.M.; Chen, Z.H.; Jing, J.P.; Lu, G.Y.; Feng, C. Boosted photoinduced cathodic protection performance of $ZnIn_2S_4/TiO_2$ nanoflowerbush with efficient photoelectric conversion in NaCl solution. *J. Alloys Compd.* **2021**, *876*, 160144. [CrossRef]
40. Jin, P.; Guan, Z.C.; Wang, H.P.; Wang, X.; Song, G.L.; Du, R.G. Fabrication of CdSe/$ZnIn_2S_4$ modified TiO_2 nanotube composite and its application in photoelectrochemical cathodic protection. *J. Electroanal. Chem.* **2022**, *904*, 115884. [CrossRef]
41. Ma, Z.; Ma, X.M.; Wang, X.T.; Liu, N.Z.; Liu, X.H.; Hou, B.R. Study on the Photocathodic Protection of Q235 Steel by $CdIn_2S_4$ Sensitized TiO_2 Composite in Splash Zone. *Catalysts* **2019**, *9*, 1067. [CrossRef]
42. Stankovich, S.; Dikin, D.A.; Dommett, G.H.B.; Kohlhaas, K.M.; Zimney, E.J.; Stach, E.A.; Piner, R.D.; Nguyen, S.T.; Ruoff, R.S. Graphene-based composite materials. *Nature* **2006**, *442*, 282–286. [CrossRef]
43. Shen, Q.Q.; Wang, Y.; Xue, J.B.; Gao, G.X.; Liu, X.G.; Jia, H.S.; Li, Q.; Xu, B.S. The dual effects of RGO films in TiO_2/CdSe heterojunction: Enhancing photocatalytic activity and improving photocorrosion resistance. *Appl. Surf. Sci.* **2019**, *481*, 1515–1523. [CrossRef]
44. Li, H.; Wang, X.T.; Zhang, L.; Hou, B.R. CdTe and graphene co-sensitized TiO_2 nanotube array photoanodes for protection of 304SS under visible light. *Nanotechnology* **2015**, *26*, 155704. [CrossRef]
45. Cao, W.C.; Wang, W.C.; Yang, Z.X.; Wang, W.H.; Chen, W.G.; Wu, K.C. Enhancing photocathodic protection performance by controlled synthesis of Bi/BiOBr/TiO_2 NTAs Z-scheme heterojunction films. *J. Alloys Compd.* **2023**, *960*, 170675. [CrossRef]
46. Li, H.; Song, W.Z.; Cui, X.Q.; Li, Y.H.; Hou, B.R.; Zhang, X.P.; Wang, Y.Q.; Cheng, L.J.; Zhang, P.F.; Li, J.R. $AgInS_2$ and graphene co-sensitized TiO_2 photoanodes for photocathodic protection of Q235 carbon steel under visible light. *Nanotechnology* **2020**, *31*, 305704. [CrossRef]
47. Hu, J.; Zhu, Y.F.; Liu, Q.; Gao, Y.B.; Du, R.G.; Lin, C.J. SnO_2 Nanoparticle Films Prepared by Pulse Current Deposition for Photocathodic Protection of Stainless Steel. *J. Electrochem. Soc.* **2015**, *162*, C161–C166. [CrossRef]
48. Zhu, J.K.; Li, H.; Cui, X.Q.; Yang, Z.Y.; Chen, B.; Li, Y.H.; Zhang, P.F.; Li, J.R. Efficient photocathodic protection performance of $ZnIn_2S_4$ nanosheets/SnO_2 quantum dots/TiO_2 nanotubes composite for 316 SS under visible light. *J. Alloys Compd.* **2022**, *926*, 166901. [CrossRef]
49. Zhu, J.K.; Li, H.; Yang, Z.Y.; Li, Y.H.; Zhang, P.F. $CaIn_2S_4$ nanosheets and SnO_2 nanoflowers co-sensitized TiO_2 nanotubes photoanode for continuous and efficient photocathodic protection of Q235 carbon steel. *J. Alloys Compd.* **2024**, *970*, 172570. [CrossRef]
50. Liang, Y.; Guan, Z.C.; Wang, H.P.; Du, R.G. Enhanced photoelectrochemical anticorrosion performance of WO_3/TiO_2 nanotube composite films formed by anodization and electrodeposition. *Electrochem. Commun.* **2017**, *77*, 120–123. [CrossRef]
51. Yang, Y.Y.; Chen, Z.Y.; Feng, C.; Jing, J.P. The $CdIn_2S_4/WO_3$ Nanosheet Composite Has a Significantly Enhanced Photoelectrochemical Cathodic Protection Performance and Excellent Electron Storage Capability. *Chem. Eur. J.* **2021**, *27*, 11589–11599. [CrossRef]
52. Tian, J.; Chen, Z.Y.; Ma, L.; Hou, J.; Feng, C.; Jing, J.P.; Sun, M.M.; Chen, D.C. Fabrication of flower-like $WO_3/ZnIn_2S_4$ composite with special electronic transmission channels to improve carrier separation for photoinduced cathodic protection and electron storage. *Appl. Surf. Sci.* **2023**, *607*, 155019. [CrossRef]
53. Zhu, J.K.; Zhang, X.; Yang, Z.Y.; Zhang, X.Y.; Li, Y.H.; Li, D.; Li, H. Enhancing photocathodic protection of Q235 carbon steel by co-sensitizing TiO_2 nanotubes with $CdIn_2S_4$ nanogranules and WO_3 nanoplates. *J. Alloys Compd.* **2024**, *976*, 173184. [CrossRef]
54. Samsudin, M.F.R.; Ullah, H.; Tahir, A.A.; Li, X.H.; Ng, Y.H.; Sufian, S. Superior photoelectrocatalytic performance of ternary structural $BiVO_4$/GQD/g-C_3N_4 heterojunction. *J. Colloid Interface Sci.* **2021**, *602*, 900. [CrossRef]
55. Li, J.S.; Chu, Y.X.; Zhang, C.Q.; Zhang, X.; Wu, C.Q.; Xiong, X.Q.; Zhou, L.J.; Wu, C.L.; Han, D.M. CoFe prussian blue decorated $BiVO_4$ as novel photoanode for continuous photocathodic protection of 304 stainless steel. *J. Alloys Compd.* **2021**, *887*, 161279. [CrossRef]

56. Yang, Z.Y.; Li, H.; Cui, X.Q.; Zhu, J.K.; Li, Y.H.; Zhang, P.F.; Li, J.R. Direct Z-scheme nanoporous $BiVO_4$/CdS quantum dots heterojunction composites as photoanodes for photocathodic protection of 316 stainless steel under visible light. *Appl. Surf. Sci.* **2022**, *603*, 154394. [CrossRef]
57. Yang, Z.Y.; Li, H.; Zhu, J.K.; Li, W.T.; Li, Y.H.; Zhang, P.F. Preparation of ZIF-67/$BiVO_4$ composite photoanode and its enhanced photocathodic protection performance of 316 SS under visible light. *J. Alloys Compd.* **2023**, *961*, 170926. [CrossRef]
58. Chen, F.W.; Jian, D.H.; Liu, S.Q.; Li, S.Y.; Wu, S.; Song, Y.H.; Liu, B. Energy-storing WO_3@$BiVO_4$ composite as photocathodic protective coatings. *Mater. Chem. Phys.* **2023**, *305*, 127987. [CrossRef]
59. Guo, H.X.; Zhang, Y.R.; Wang, S.; Li, L.L.; Wang, W.M.; Sun, Q.S. In-situ generation of Bi_2S_3 to construct WO_3/$BiVO_4$/Bi_2S_3 heterojunction for photocathodic protection of 304SS. *J. Electroanal. Chem.* **2022**, *907*, 116033. [CrossRef]
60. Zheng, H.G.; Sun, X.; Liu, Y.; Jiang, S.Y.; Wang, D.R.; Fan, Y.K.; Hu, L.L.; Zhang, D.Q.; Yao, W.F.; Zhang, L.Z. New g-C_3N_4/GO/MoS_2 composites as efficient photocatalyst for photocathodic protection of 304 stainless steel. *Water Sci. Technol.* **2021**, *84*, 499–511. [CrossRef]
61. Zhao, M.X.; Yang, X.L.; Li, X.Y.; Tang, Z.; Song, Z.W. Photocathodic protection performance of Ni_3S_2/g-C_3N_4 photoanode for 304 stainless steel. *J. Electroanal. Chem.* **2021**, *893*, 115324. [CrossRef]
62. Ding, D.; Hou, Q.K.; Su, Y.G.; Li, Q.Q.; Liu, L.; Jing, J.; Lin, B.; Chen, Y. g-C_3N_4/TiO_2 hybrid film on the metal surface, a cheap and efficient sunlight active photoelectrochemical anticorrosion coating. *J. Mater. Sci. Mater. Med.* **2019**, *30*, 12710–12717. [CrossRef]
63. Zheng, H.; Liu, Y.; Zhou, Y.H.; Zhao, D.L.; Wang, D.R.; Yun, L.; Zhang, D.Q.; Zhang, L.Z. Improved photocathodic protection performance of g-C_3N_4/rGO/ZnS for 304 stainless steel. *J. Phys. Chem. Solids* **2021**, *148*, 109672. [CrossRef]
64. Zhang, Y.M.; Bao, H.; Liu, X.Y.; Zhang, X.Y.; He, H.Y.; Li, T.Y.; Yang, H.; Shah, S.P.; Li, W.H. Bi_2S_3 nanoparticles/ZnO nanowire heterojunction films for improved photoelectrochemical cathodic protection for 304 SS under visible light. *J. Appl. Electrochem.* **2022**, *52*, 559–571. [CrossRef]
65. Lin, Y.C.; Liu, S. Robust ZnO nanowire photoanodes with oxygen vacancies for efficient photoelectrochemical cathodic protection. *Appl. Surf. Sci.* **2021**, *566*, 150694. [CrossRef]
66. Feng, C.; Chen, Z.Y.; Tian, J.; Jing, J.P.; Ma, L.; Hou, J. Fabrication of three-dimensional WO_3/$ZnWO_4$/ZnO multiphase heterojunction system with electron storage capability for significantly enhanced photoinduced cathodic protection performance. *J. Mater. Sci. Technol.* **2021**, *90*, 183–193. [CrossRef]
67. Yang, Y.; Cheng, W.; Cheng, Y.F. Preparation of Co_3O_4@ZnO core-shell nanocomposites with intrinsic p-n junction as high-performance photoelectrodes for photoelectrochemical cathodic protection under visible light. *Appl. Surf. Sci.* **2019**, *476*, 815–821. [CrossRef]
68. Helal, A.; Jianqiang, Y.; Eid, A.I.; El-Hakam, S.A.; Samra, S.E.; El-Sheikh, S.M. A novel g-C_3N_4/In_2O_3/$BiVO_4$ heterojunction photoanode for improved the photoelectrochemical cathodic protection of 304 SS stainless steel under solar light. *J. Alloys Compd.* **2022**, *911*, 165047. [CrossRef]
69. Zhang, Y.; Yu, J.Q.; Sun, K.; Zhu, Y.K.; Bu, Y.Y.; Chen, Z.Y. Indium oxide thin film as potential photoanodes for corrosion protection of stainless steel under visible light. *Mater. Res. Bull.* **2014**, *53*, 251–256. [CrossRef]
70. Kong, L.N.; Tang, X.X.; Du, X.R.; Xie, Z.H.; Wang, X.X.; Xie, Q.; Wang, J.M.; Cai, J.J. Surface engineering of TiO_2@$SrTiO_3$ heterojunction with Ni_2S_3 for efficient visible-light-driven photoelectrochemical cathodic protection. *J. Alloys Compd.* **2022**, *927*, 166861. [CrossRef]
71. Kong, C.H.; Su, X.Y.; Qing, D.; Zhao, Y.N.; Wang, J.S.; Zeng, X.F. Controlled synthesis of various SrTiO3 morphologies and their effects on photoelectrochemical cathodic protection performance. *Ceram. Int.* **2022**, *48*, 20228–20236. [CrossRef]
72. Jing, J.P.; Chen, Z.Y.; Bu, Y.Y.; Sun, M.M.; Zheng, W.Q.; Li, W.B. Significantly enhanced photoelectrochemical cathodic protection performance of hydrogen treated Cr-doped $SrTiO_3$ by Cr^{6+} reduction and oxygen vacancy modification. *Electrochim. Acta* **2019**, *304*, 386–395. [CrossRef]
73. Yang, Y.; Cheng, Y.F. Bi-layered CeO_2/$SrTiO_3$ nanocomposite photoelectrode for energy storage and photocathodic protection. *Electrochim. Acta* **2017**, *253*, 134–141. [CrossRef]

Disclaimer/Publisher's Note: The statements, opinions and data contained in all publications are solely those of the individual author(s) and contributor(s) and not of MDPI and/or the editor(s). MDPI and/or the editor(s) disclaim responsibility for any injury to people or property resulting from any ideas, methods, instructions or products referred to in the content.